Journal for ImmunoTherapy of Cancer

Nuclear imaging-guided PD-L1 blockade therapy increases effectiveness of cancer immunotherapy

Hannan Gao,[1] Yue Wu,[1] Jiyun Shi ,[2] Xin Zhang,[1] Tianyu Liu,[1] Biao Hu,[1] Bing Jia,[1] Yakun Wan,[3] Zhaofei Liu,[1] Fan Wang[1,2,4]

To cite: Gao H, Wu Y, Shi J, *et al*. Nuclear imaging-guided PD-L1 blockade therapy increases effectiveness of cancer immunotherapy. *Journal for ImmunoTherapy of Cancer* 2020;**8**:e001156. doi:10.1136/jitc-2020-001156

► Additional material is published online only. To view, please visit the journal online (http://dx.doi.org/10.1136/jitc-2020-001156).

HG, YW and JS contributed equally.

Accepted 16 October 2020

[1]Medical Isotopes Research Center and Department of Radiation Medicine, State Key Laboratory of Natural and Biomimetic Drugs, School of Basic Medical Sciences, Peking University, Beijing, China
[2]Key Laboratory of Protein and Peptide Pharmaceuticals, CAS Center for Excellence in Biomacromolecules, Institute of Biophysics, Chinese Academy of Sciences, Beijing, China
[3]Shanghai Novamab Biopharmaceuticals Co., Ltd, Shanghai, China
[4]Bioland Laboratory (Guangzhou Regenerative Medicine and Health Guangdong Laboratory), Guangzhou, China

Correspondence to
Professor Fan Wang;
wangfan@bjmu.edu.cn

ABSTRACT

Objectives Strategies to improve the responsiveness of programmed death-1 (PD-1)/programmed death ligand-1 (PD-L1) checkpoint blockade therapy remain an essential topic in cancer immunotherapy. In this study, we developed a new radiolabeled nanobody-based imaging probe ^{99m}Tc-MY1523 targeting PD-L1 for the enhanced therapeutic efficacy of PD-L1 blockade immunotherapy by the guidance of ^{99m}Tc-MY1523 SPECT/CT imaging.

Methods The binding affinity and specificity of nanobody MY1523 were measured in vitro. MY1523 was radiolabeled with ^{99m}Tc by a site-specific transpeptidation of Sortase-A, and the biodistribution and single photon emission CT (SPECT)/CT were performed in mice bearing different tumors. We used interferon-γ (IFN-γ) as an intervention means to establish animal models with different levels of PD-L1 expression, then investigated the ability of ^{99m}Tc-MY1523 SPECT/CT for the in vivo non-invasive measurement of PD-L1 expression in tumors. Finally, the PD-L1 blockade immunotherapies guided by ^{99m}Tc-MY1523 SPECT/CT were carried out in MC-38, A20, and 4T1 tumor-bearing mouse models, followed by the testing of tumor infiltration T cells.

Results MY1523 exhibited a high binding affinity and specificity to PD-L1 and had no competitive binding with the therapeutic antibody. ^{99m}Tc-MY1523 was prepared with high specific activity and radiochemical purity. It was found that tumor PD-L1 expression was dynamically upregulated by IFN-γ intervention in MC-38, A20, and 4T1 tumor-bearing mouse models, as indicated by ^{99m}Tc-MY1523 SPECT/CT. The PD-L1 blockade therapy initiated during the therapeutic time window determined by ^{99m}Tc-MY1523 SPECT/CT imaging significantly enhanced the therapeutic efficacy in all animal models, while the tumor growth was effectively suppressed, and the survival time of mice was evidently prolonged. A correlation between dynamically upregulated PD-L1 expression and improved PD-L1 blockade therapy effectiveness was revealed, and the markedly increased infiltration of effector T cells into tumors was verified after the imaging-guided therapy.

Conclusion Our results demonstrated that ^{99m}Tc-MY1523 SPECT/CT allowed a real-time, quantitative and dynamic mapping of PD-L1 expression in vivo, and the imaging-guided PD-L1 blockade immunotherapy significantly enhanced the therapeutic efficacy. This strategy merits translation into clinical practice for the better management of combination therapies with radiotherapy or chemotherapy.

INTRODUCTION

Although programmed death-1 (PD-1) or programmed death ligand-1 (PD-L1) checkpoint blockade has been a breakthrough in cancer therapy,[1 2] the objective response rate in solid tumors is only 20% to 30%.[3 4] Therefore, strategies to improve the responsiveness of PD-1/PD-L1 blockade therapy remain an essential topic in cancer immunotherapy.[5] The interaction between PD-1 and PD-L1 inhibits the function of effector T cells and the priming of naïve T cells, leading to impaired antitumor immunity.[6 7] It has been reported that PD-L1 expression is an important biomarker for guiding effector T-cell-based cancer immunotherapy.[8 9]

Immunohistochemistry (IHC) of tumor tissues obtained from invasive procedures such as biopsy and surgery are currently the most commonly used method to determine the PD-L1 expression levels.[10 11] However, the PD-L1 expression in tumors is a dynamic process and it can be regulated by several cytokines such as interferon-γ (IFN-γ) and also by treatment strategies such as radiotherapy.[12 13] Therefore, IHC cannot be used to dynamically detect changes of PD-L1 expression in clinical practice.[14 15] In addition, there are no strict criteria to define the positivity or negativity of PD-L1 expression by IHC, and the PD-L1 levels determined by IHC might not represent the actual status due to the tumor heterogeneity.[16] It has been reported that the predictive accuracy of IHC is generally <30%.[17 18] In contrast to IHC, non-invasive imaging of PD-L1 expression in tumors can determine the PD-L1 levels in a real time, dynamic and quantitative manner, which would be beneficial to guide cancer immunotherapy.[19]

Recently, molecular imaging of PD-L1 expression with single photon emission CT (SPECT) and positron emission tomography (PET) based on the traditional radiolabeled

antibodies, such as ^{111}In-10B5, ^{89}Zr-pembrolizumab, ^{89}Zr-nivolumab, ^{68}Ga/^{64}Cu-DOTA-HACA-PD1 and ^{64}Cu-PD-L1 mAb, have been investigated for preclinical and clinical applications.[20–24] However, challenges remain for antibody-based imaging probes in the dynamic imaging due to slow clearance of antibodies from the blood stream and normal tissues. It usually takes 1 to 3 days for antibody-based probes to reach a favorable contrast, which hindered their wide clinical application. In contrast to intact antibody, single-domain nanobodies have much better tissue permeability and faster metabolism, resulting in high tumor contrast at much earlier time point of 1 to 2 hours post injection (p.i.).[25–27] Moreover, the site-specific radiolabeling of nanobodies by a transpeptidase of Sortase-A would lead to easy quality control of reproducibility.[28]

In this study, we hypothesized that SPECT imaging-guided PD-L1 blockade therapy would increase the therapeutic effectiveness and tried to find an optimal time point or time interval by SPECT/CT imaging to perform the PD-L1 blockade therapy. Therefore, we developed a new radiolabeled nanobody ^{99m}Tc-MY1523 targeting PD-L1. SPECT/CT was performed in mice bearing different tumors to monitor dynamically upregulated PD-L1 expression after IFN-γ intervention. Furthermore, we also carried out therapy studies guided by ^{99m}Tc-MY1523 SPECT/CT and established a direct correlation between dynamically upregulated PD-L1 expression and improved PD-L1 blockade therapy effectiveness.

MATERIALS AND METHODS

Cells and animal models

MC-38 and A20 tumor cells were kindly provided by Yangxin Fu at Institute of Biophysics, Chinese Academy of Sciences (Beijing, China). The 4T1 tumor cells were purchased from the American Type Culture Collection (Manassas, Virginia, USA). Cells were cultured in Roswell Park Memorial Institute-1640 (RPMI-1640) or Dulbecco's Modified Eagle Medium (DMEM) medium with 10% fetal bovine serum in a humidified atmosphere with 5% CO_2 at 37°C. Female C57/BL6 and BALB/c mice of 5 to 6 weeks age were purchased from Vital River Laboratory Animal Technology Co, Ltd (Beijing, China). To prepare syngenetic tumor models, A20 or 4T1 tumor cells (1×10^6 cells) were inoculated subcutaneously into the right flank of BALB/c mice, and MC-38 tumor cells (1×10^6 cells) were inoculated subcutaneously into the right flank of C57/BL6 mice.

Preparation of ^{99m}Tc-MY1523

The murine PD-L1-targeted nanobody MY1523, which has a LPETG-His_6 tag on the C-terminus for both Ni-sepharose purification and site-specific transpeptidation reaction of Sortase-A, was provided by Novamab Biopharmaceuticals Co, Ltd (Shanghai, China). The two-step labeling approach was adopted for the preparation of ^{99m}Tc-MY1523. First, we prepared ^{99m}Tc-HYNIC-G_4K (HYNIC=6-hydrazinonicotinyl, G_4K=Gly-Gly-Gly-Gly-Lys). The mixture of 3 µg G_4K(HYNIC)-OH (GL Biochem Ltd, Shanghai, China), 5 mg TPPTS (trisodium triphenylphosphine-3,3′,3″-trisulfonate, J&K Chemical Ltd, Beijing, China), 6.5 mg tricine (J&K Chemical Ltd, Beijing, China) and 74 to 96 MBq $Na^{99m}TcO_4$ (HTA Co, Ltd, Beijing, China) were reacted in 200 µL succinate buffer (250 mM, pH=4.8) at 99°C for 15 min. Then, the pH of the solution was adjusted to 7 to 8 by 2M NaOH. Second, we prepared ^{99m}Tc-MY1523 by labeling MY1523 with ^{99m}Tc-HYNIC-G_4K. The mixture of 74 MBq ^{99m}Tc-HYNIC-G_4K, 100 µg MY1523, 50 µg Sortase-A (Detai Biologics Co, Ltd, Nanjing, China) and 10 µL $CaCl_2$ (1M) were reacted at room temperature (RT) for 20 min. The product was purified by high-performance size exclusion chromatography (HPSEC) (Superose 12, 10×300 mm, GE Healthcare Life Science) or Superdex-75 (Increase 10/300 GL, GE Healthcare Life Science) using phosphate-buffered saline (PBS) containing 0.1% Tween-20 (pH=7.4) as the eluent, and the flow rate was 0.8 mL/min. The radiochemical purity of ^{99m}Tc-MY1523 was determined using instant thin layer chromatography-silica gel (ITLC-SG, Agilent, USA) developed in saline, then detected via a radio-TLC imaging scanner (Bioscan, AR-2000, USA). Rf values were 0.7 to 1 for $Na^{99m}TcO_4$ and ^{99m}Tc-HYNIC-G_4K, and 0 to 0.3 for ^{99m}Tc-MY1523. The cold MY1523 was added into injection doses to obtain a specific activity of 2.7 MBq/nmol for both SPECT/CT imaging and biodistribution. The more detailed radiochemistry properties of ^{99m}Tc-HYNIC-G_4K and ^{99m}Tc-MY1523 are provided in the supporting information.

PD-L1 receptor binding assays

The binding affinity and specificity of MY1523 was determined by receptor binding assay using ^{125}I-MY1523 as the radiotracer. To prepare ^{125}I-labeled MY1523, the mixture of MY1523 and $Na^{125}I$ (Perkin Elmer Inc, USA) and PBS (0.1M, pH=7.4) was reacted in a glass vial coated with 30 µg 1,3,4,6-Tetrachloro-3α,6α-diphenylglycouril (Iodo-Gen, Sigma, USA) at RT for 2 min, resulting in a product with high specific activity (~10.3 MBq/nmol) and radiolabeling yield (>95%) tested by ITLC-SG (Agilent, USA).

The PD-L1 binding assays were performed on 96-well ELISA plates coated with 0.2 µg/well recombinant murine PD-L1 (Sino Biological, Cat: 50010-M08H, China). For the saturation binding assay, a gradient of ^{125}I-MY1523 (1 to 200 nM) were added to the plates and incubated at RT for 2 hours. For receptor competitive binding assay, a gradient of cold MY1523 or anti-PD-L1 (αPD-L1) antibody (clone: 10F.9G2, BioXcell) (0.1 to 3000 nM) was incubated with ^{125}I-MY1523 (1 nM) at RT for 2 hours. After several washes with PBS, the plates were counted for radioactivity in each cell via an automatic γ-counter (PerkinElmer Inc, USA). The equilibrium dissociation constant (KD) and the best-fit 50% inhibitory concentration (IC_{50}) values were analyzed using Prism V.7.0 (GraphPad Software Inc, San Diego, Canada). Experiments were performed twice with four duplicates. The binding of ^{99m}Tc-MY1523 to A20

cells were also determined, and the result is shown in the supporting information.

IFN-γ intervention

For in vitro treatment, MC-38, A20 and 4T1 tumor cells were incubated with 200 IU/mL recombinant murine IFN-γ (Peprotech, Rocky Hill, USA) in the complete medium at 37°C for 24 hours, and then the cells were harvested, stained with PD-L1 (1 µg/mL, Cat. 12-5982-82, eBioscience) at 4°C for 30 min and analyzed by a flow cytometer (Calibur, BD Biosciences, USA) to determine the changes of PD-L1 expression on tumor cells. For in vivo treatment, the tumor-bearing mice were injected intratumorally (i.t.) with 1000 IU IFN-γ daily for 5 days. The dynamically changed PD-L1 expression in tumors was determined by SPECT/CT imaging and verified by the flow cytometry, while the PD-L1 expression was reported as median fluorescence intensity (MFI).

Biodistribution

Biodistribution studies were performed in MC-38 tumor-bearing mice, which were injected intravenously with 190 kBq ^{99m}Tc-MY1523 and sacrificed at 1, 2 and 4 hours p.i., respectively (n=4). To verify the in vivo specificity of ^{99m}Tc-MY1523, mice in the blocking group were co-injected with 200 µg cold MY1523 and sacrificed at 2 hours p.i. Samples of blood, tumor, normal tissues and organs were harvested, weighted and counted via a γ-counter. The uptake was expressed as percentage of injected dose per gram (%ID/g).

SPECT/CT

SPECT/CT was performed in mice bearing MC-38, A20 or 4T1 tumors. The mice were injected intraveneously with 18 MBq ^{99m}Tc-MY1523, anesthetized by inhaling 1.5% isoflurane, and imaged at 2 hours p.i. (n=4) using the NanoScan SPECT/CT system (Mediso Ltd, Hungary): pinhole SPECT (peak: 140 keV, 20% width; frame time: 25 s), helical CT (50 kVp, 0.67 mA, rotation 210°, exposure time: 300 ms). SPECT and CT images were merged using the Nucline software V.2.0 (Mediso Ltd.). The regions of interest were drawn for the determination of tumor sizes (mm^3) and radioactivity (Bq), then the tumor uptake was calculated as percentage injected dose per volume (%ID/cc). Immediately after SPECT scanning, the mice treated with and without IFN-γ were sacrificed to testify the tumor PD-L1 expression by flow cytometry. The linear coefficient between the tumor uptake of ^{99m}Tc-MY1523 and the PD-L1 expression (MFI) either on tumor cells or dendritic cells (DCs) was determined (n=4 for PBS group and IFN-γ group each).

Imaging-guided PD-L1 blockade therapy

Imaging-guided PD-L1 blockade therapies were performed in MC-38, A20 and 4T1 tumor models. The mice were injected i.t. with PBS or IFN-γ from day 4 after tumor cell inoculation for 5 days, and then were subjected to SPECT/CT imaging to determine the dynamic PD-L1 expression in tumors on day 8 and 12 after tumor cell inoculation. When the tumor uptake of ^{99m}Tc-MY1523 was observed to be apparently increased by SPECT/CT, the mice were injected intraperitoneally with 200 µg αPD-L1 antibody (clone: 10F.9G2, BioXcell) twice with 4 days interval, while using PBS, IFN-γ and αPD-L1 antibody 10F.9G2 without IFN-γ intervention as controls (n=5 for therapy studies, and n=8 for flow cytometry). Tumor sizes were measured twice a week and calculated as volumes (mm^3)=length×width×height/2. Mice were sacrificed when tumor size was greater than 1200 mm^3.

To analyze tumor infiltration of T cells, the mice were sacrificed and tumors were excised for flow cytometry, while the mice in PBS group and IFN-γ group were sacrificed on day 8 and 16 after tumor cell inoculation, as well as the mice in αPD-L1 antibody groups with and without IFN-γ intervention were sacrificed on day 16 and 35 after tumor cell inoculation (n=4 at each time point), respectively. The results were shown as the percentage of CD8$^+$ or CD4$^+$ T cells in digested tumor cells. We also determined the Treg cells in tumors as well as the activated effector T cells in tumor draining lymph nodes, and the information is provided in the supporting information.

Flow cytometry

The tumor tissues were diced and digested in PBS containing 1 mg/mL collagenase-IV (Worthington Bio, Lakewood, USA), 0.1 mg/mL DNase-I (Roche, Mannheim, Germany) and 2% fetal bovine serum at 37°C for 1 to 2 hours. Single cell suspension was obtained through 80 mesh-sized cell sieve. To block Fc receptor on immune cells, the cells were incubated with CD16/32 (10 µg/mL, clone 2.4G2, BioXcell) at 4°C for 10 min before staining. To analyze PD-L1 expression on tumor cells (CD45$^-$ for MC-38 and 4T1 tumor cells, and CD19$^+$ for A20 tumor cells) and DCs (CD45$^+$CD11c$^+$MHCII$^+$), the cells were incubated with CD45 (1 µg/mL, Cat. 56-0451-82, eBioscience), CD19 (1 µg/mL, Cat. 115512, Biolegend), CD11c (1 µg/mL, Cat. 15-0114-82), MHC-II (1 µg/mL, Cat. 25-5321-82, eBioscience) and PD-L1 (1 µg/mL, Cat. 12-5982-82, eBioscience) antibodies at 4°C for 30 min. To analyze tumor infiltration numbers of CD8$^+$ T cells (CD45$^+$CD3e$^+$CD8$^+$) and CD4$^+$T cells (CD45$^+$CD3e$^+$CD4$^+$), the cells were incubated with CD45 (1 µg/mL), CD3e (1 µg/mL, Cat. 25-0031-82, eBioscience), CD4 (1 µg/mL, Cat. 45-0042-82, eBioscience) and CD8a (2.5 µg/mL, Cat. 11-0081-82, eBioscience) antibodies at 4°C for 30 min. Samples were analyzed via a FACS Calibur (BD Biosciences, USA) or Gallios (Beckman Coulter, USA) flow cytometer.

Immunofluorescence staining

Frozen sections of MC-38 tumor (10 µm) were fixed by 4% paraformaldehyde and blocked with 5% bovine serum albumin in PBS. MY1523 (10 µg/mL) and rabbit anti-murine PD-L1 antibody (1:100, Abcam, Cat. ab80276) were first incubated with the tumor sections at 4°C overnight. Then, Dylight 650 conjugated mouse anti-His$_6$-tag IgG (1:500, Abcam, Cat. ab117504) and Dylight-488

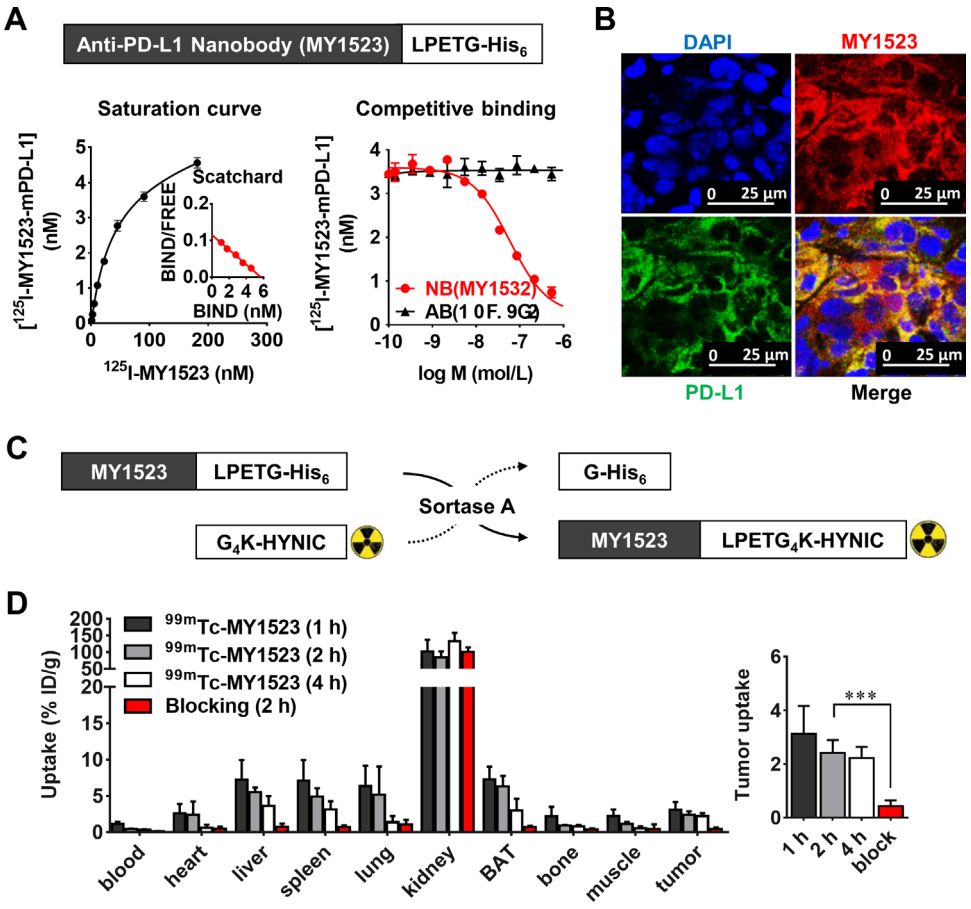

Figure 1 Murine PD-L1-specific targeting of nanobody MY1523 and biodistribution of ^{99m}Tc-MY1523. MY1523 was expressed with a nanobody sequence targeting to murine PD-L1 and a LPETG-His$_6$ tag on the C-terminus. (A) The saturation binding curve of ^{125}I-MY1523 and the competitive binding curves of nanobody MY1523 and antibody 10F.9G2 against ^{125}I-MY1523 (n=4, mean±SD). (B) Immunofluorescence staining of PD-L1 on MC-38 tumor sections. (C) The radiochemical strategy to prepare ^{99m}Tc-MY1523 by site-specific Sortase-A transpeptidation from ^{99m}Tc-HYNIC-G$_4$K to LPETG-His$_6$ tagged MY1523. (D) Biodistribution of ^{99m}Tc-MY1523 in MC-38 tumor-bearing mice with or without blocking (n=4, mean±SD, ***p<0.001). BAT, brown adipose tissue; PD-L1, programmed death ligand-1.

conjugated goat-anti-rabbit IgG (1:500, Abbkine, Cat. A23220) were incubated at RT for 2 hours. For nucleus staining, DAPI (20 ug/mL) was stained for 5 min. The immunofluorescence images were captured via a TCS SP8 confocal microscope (Leica, Wetzlar, Germany).

Statistical analysis

Data were analyzed using Prism V.7.0 (GraphPad Software Inc, San Diego, Canada) and represented as the mean±SD. Statistics were performed using Student t-test assuming unequal variances. A p value of <0.05 was considered statistically significant.

RESULTS

PD-L1-targeting specificity of MY1523

The PD-L1-targeting specificity of MY1523 was determined by the protein binding assay and immunofluorescence staining. As shown in figure 1A, MY1523 exhibited a high binding affinity (KD=49.70±7.90 nM) and specificity (IC_{50}=59.23±0.04 nM) to PD-L1 and had no competitive binding with the antibody 10F.9G2 (IC_{50}>10 μM). The immunofluorescence staining showed co-localization of MY1523 on PD-L1 expressed in MC-38 tumor tissues (figure 1B). The isotype control staining is provided in supporting information (online supplemental figure S1). These results revealed that MY1523 specifically targeted PD-L1.

Preparation and in vivo evaluation of ^{99m}Tc-MY1523

^{99m}Tc-MY1523 was prepared by a site-specific transpeptidation of Sortase-A (figure 1C). The labeling yield of ^{99m}Tc-HYNIC-G$_4$K was >95%, and the total labeling yield for ^{99m}Tc-MY1523 was ~50% (online supplemental figure S2A,B). The radiochemical purity of the final product was >99% after purification (online supplemental figure S2C). The HPSEC and sodium dodecyl sulfate polyacrylamide gel electrophoresis results of ^{99m}Tc-MY1523 were consistent to that of ITLC (online supplemental figure S3A,B). In the resulting solution, ^{99m}Tc-MY1523 was proved to be stable for 6 hours at RT (online supplemental figure S2D). The binding affinity

of ^{99m}Tc-MY1523 was determined on A20 cells, and the IC_{50} was determined to be 5.95±0.71 nM (online supplemental figure S3C).

The biodistribution of ^{99m}Tc-MY1523 was determined in mice bearing MC-38 tumors. The results showed fast blood clearance, renal-route excretion and satisfactory tumor uptake of ^{99m}Tc-MY1523 (figure 1D). The blood radioactivity was 1.15±0.25, 0.45±0.05, and 0.31%±0.08%ID/g at 1, 2 and 4 hours p.i., respectively. The kidney uptake was 102.00±35.49, 84.05±18.44 and 133.49%±24.84%ID/g at 1, 2 and 4 hours p.i., respectively. The brown adipose tissue uptake was 7.29±1.74, 6.32±1.44 and 2.98%±1.61%ID/g at 1, 2 and 4 hours p.i., respectively. The tumor uptake was 3.12±1.04, 2.42±0.47 and 2.23%±0.41%ID/g at 1, 2 and 4 hours p.i., respectively. The tumor uptake in the blocking group was significantly lower compared with the group without blocking (0.44±0.21 vs 2.42%±0.47%ID/g, at 2 hours p.i., p<0.001), suggesting a high in vivo specificity.

Monitoring PD-L1 expression changes after IFN-γ intervention

Interferon receptor signaling pathways upregulate PD-L1 expression.[29] In this study, we used IFN-γ as an intervention means to regulate the tumor PD-L1 expression. The results from in vitro studies showed significantly upregulated PD-L1 expression by IFN-γ intervention compared with the PBS group on MC-38 (58.98±0.44 vs 24.77±1.58 MFI, p<0.0001), A20 (206.31±3.84 vs 62.53±0.16 MFI, p<0.0001) and 4T1 (48.23±4.49 vs 8.40±0.72 MFI, p<0.001) tumor cells (figure 2A). Using an IFN-γ intervention strategy (figure 2B), the in vivo imaging studies showed apparently increased tumor uptake of ^{99m}Tc-MY1523 compared with the corresponding PBS group in mice bearing MC-38 (3.17±0.37 vs 2.03%±0.12%ID/g, at 2 hours p.i., p<0.01), A20 (3.54±0.44 vs 2.68%±0.34%ID/g, at 2 hours p.i., p<0.001) and 4T1 (3.39±0.29 vs 1.63%±0.19%ID/g, at 2 hours p.i., p<0.0001) tumors (figure 2C). Subsequently, the tumors were resected to verify the imaging results. A good correlation between the

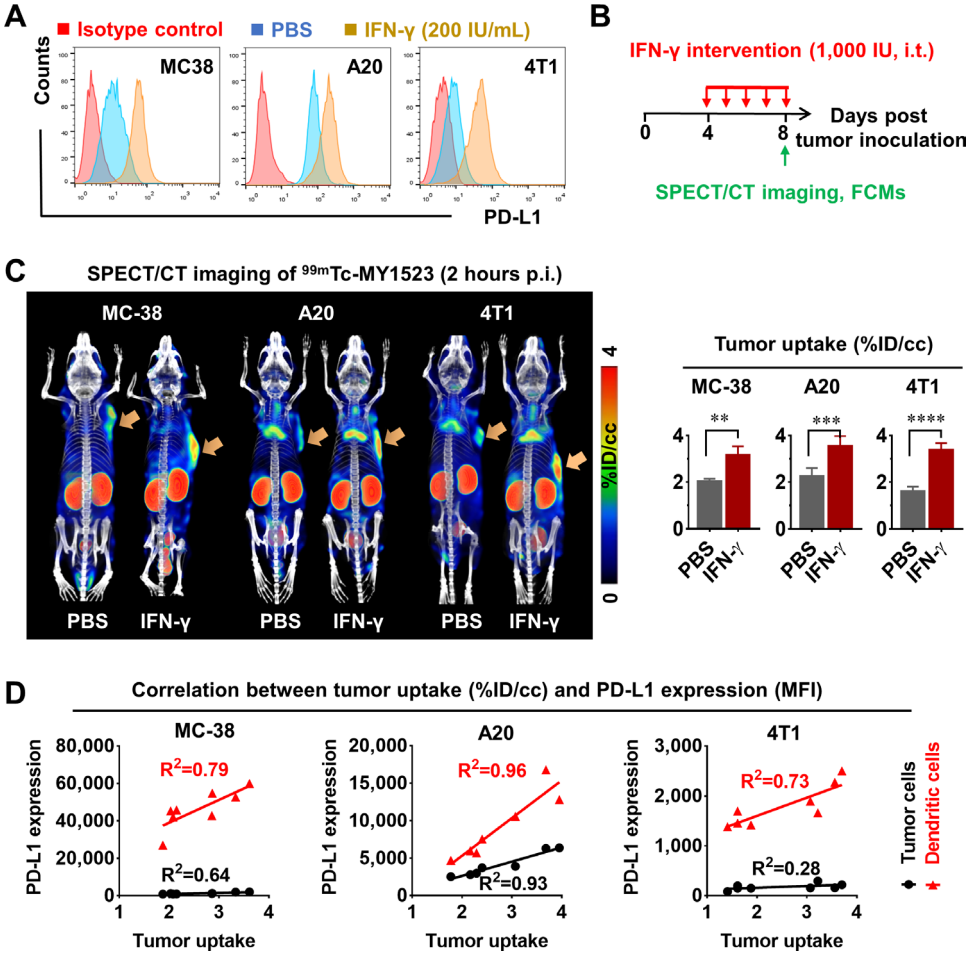

Figure 2 In vitro and in vivo PD-L1 expression changes after IFN-γ intervention. (A) The upregulated PD-L1 expression on MC-38, A20 and 4T1 tumor cells by IFN-γ intervention in vitro. (B) IFN-γ intervention strategy to regulate tumor PD-L1 expression in vivo. (C) SPECT/CT imaging and quantified tumor uptake of ^{99m}Tc-MY1523 in mice bearing MC-38, A20 and 4T1 tumors at 2 hours p.i. (n=4, mean±SD; **p<0.01, ***p<0.001, ****p<0.0001). Yellow arrows indicate tumor locations. (D) Correlation between tumor uptake of ^{99m}Tc-MY1523 and the PD-L1 expression on tumor cells and dendritic cells in MC-38, A20 and 4T1 tumors (n=4 for PBS group and IFN-γ group each). FCM, flow cytometry; IFN-γ, interferon-γ; i.t., intratumorally; MFI, median fluorescence intensity; PBS, phosphate-buffered saline; p.i., post injection; SPECT, single photon emission CT.

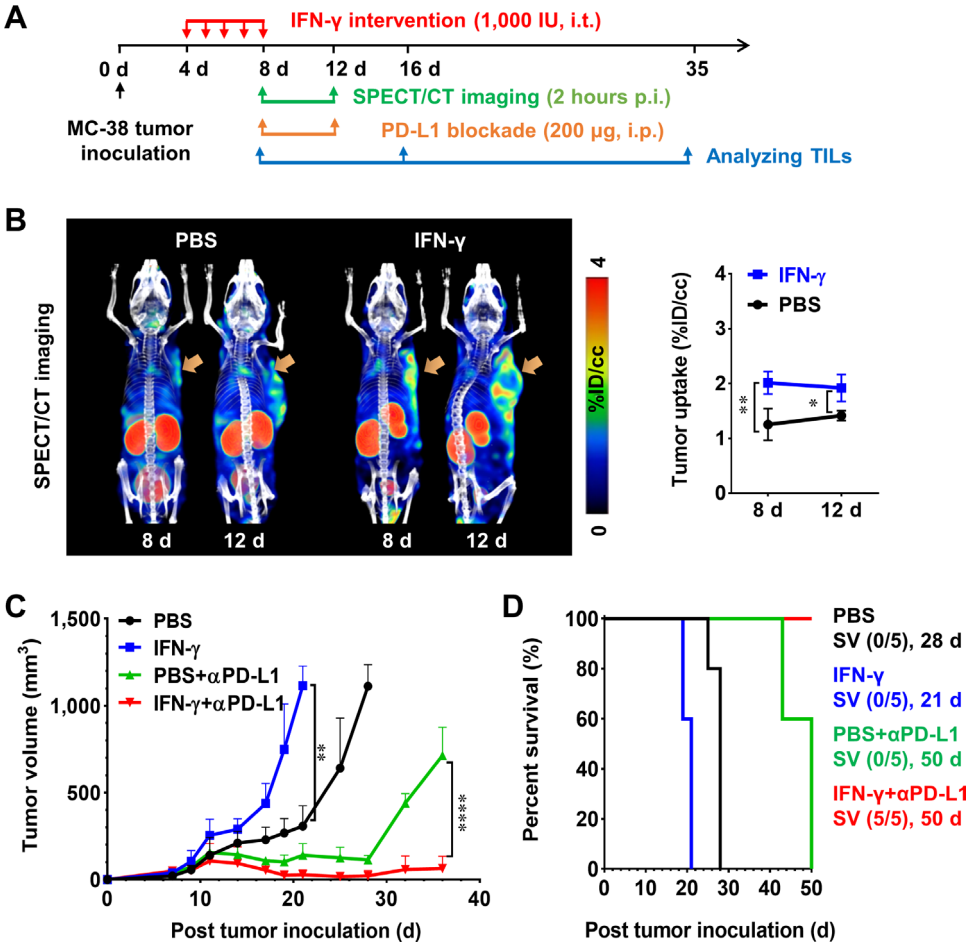

Figure 3 ^{99m}Tc-MY1523 SPECT/CT imaging-guided PD-L1 blockade therapy in MC-38 tumor-bearing mice. (A) Scheme of ^{99m}Tc-MY1523 SPECT imaging-guided PD-L1 blockade therapy. The tumor-bearing mice were administered first with IFN-γ (1000 IU, five times from day 4 to day 8, i.t.), then SPECT/CT imaging of ^{99m}Tc-MY1523 at 2 hours p.i. was performed (on day 8 and 12, intraveneously). When the PD-L1 expression was increased, the mice were treated with αPD-L1 mAb (200 μg, on day 8 and 12, i.p.), followed by the analyzes of tumor infiltration of T cells on day 8, 16 and 35. (B) SPECT/CT imaging of mice with and without IFN-γ intervention on day 8 and 12 (n=4, mean±SD; *p<0.05, **p<0.01). Yellow arrows indicate tumor locations. (C and D) Tumor growth curves (n=5, mean±SD, *p<0.05,**p<0.01, ****p<0.0001) and the Kaplan-Meier survival curves (n=5). αPD-L1, anti-programmed death ligand-1; d, days; IFN-γ, interferon-γ; i.p., intraperitoneally; i.t., intratumorally; PBS, phosphate-buffered saline; SPECT, single photon emission CT; SV, survival; TIL, tumor-infiltrating lymphocytes.

tumor uptake of ^{99m}Tc-MY1523 and the PD-L1 expression either on tumor cells or DCs was found in these three mouse models (figure 2D). These results demonstrated that ^{99m}Tc-MY1523 could be used for the in vivo non-invasive detection of PD-L1 expression in tumors.

Imaging-guided PD-L1 blockade therapy

The imaging-guided strategy was first evaluated in mice bearing MC-38 tumors as scheduled in figure 3A. When imaging results showed the upregulated PD-L1 expression in tumors after IFN-γ intervention on day 8 and 12 after tumor cell inoculation (figure 3B), the mice were subjected to PD-L1 blockade therapy. As shown in figure 3C, although IFN-γ intervention expedited the tumor growth, the imaging-guided therapy dramatically improved the therapeutic efficacy. The tumor growth was significantly suppressed, and three of five tumors completely disappeared. Compared with control groups, the survival time of mice in the treated group was also remarkably prolonged (figure 3D). All five animals in the experimental group were alive at the end of experiments (day 50 after the tumor cell inoculation), while the animals in other groups were all dead at this time point, and even at earlier time points.

To further confirm the results observed in the MC-38 tumor model, we repeated the therapy studies in A20 and 4T1 tumor models, and found that the outcome was very similar (figure 4A–D). The IFN-γ intervention also upregulated the PD-L1 expression in tumors, and the PD-L1 blockade therapy guided by ^{99m}Tc-MY1523 SPECT, which indicated the high PD-L1 expression, also remarkably improved the therapeutic efficacy. In the A20 animal model, on day 40 after the tumor cell inoculation, all five mice in the experimental group were alive, while only one mouse in the αPD-L1 antibody without IFN-γ intervention group was alive, and other mice in PBS and IFN-γ groups were all dead. Although the 4T1 tumors are

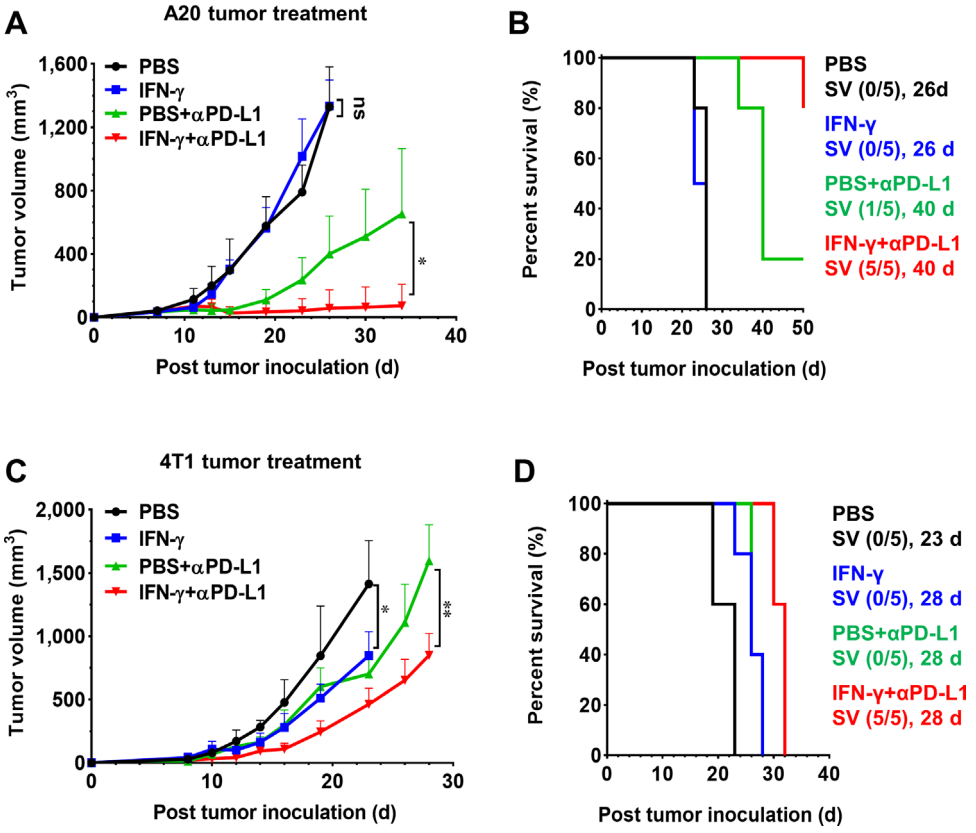

Figure 4 Imaging-guided PD-L1 blockade therapies in the mice bearing A20 and 4T1 tumors. (A and C) Tumor growth curves (n=5, mean±SD, *p<0.05, **p<0.01). (B and D) The Kaplan-Meier survival curves of mice (n=5). αPD-L1, anti-programmed death ligand-1; d, days; IFN-γ, interferon-γ; PBS, phosphate-buffered saline; SV, survival.

not sensitive to PD-L1 blockade therapy,[30 31] this strategy, upregulating the PD-L1 expression and imaging-guided PD-L1 blockade therapy, also worked well, while the tumor growth was effectively suppressed and the survival time of mice was evidently prolonged.

Tumor infiltration of T cells after treatment

In order to corroborate the results above, the percentage $CD8^+$ or $CD4^+$ T-cell infiltration in tumors was determined by flow cytometry (figure 5 and online supplemental figures S4 and S6). IFN-γ expedited MC-38 tumor growth (figure 3C), had no effect on A20 tumor growth (figure 4A) and suppressed 4T1 tumor growth (figure 4C). However, IFN-γ intervention resulted in little changes of $CD8^+$ T cells in the three kinds of tumors compared with their controls (figure 5A). A reversed correlation between $CD8^+$ T-cell infiltration and tumor growth was observed in the αPD-L1 group and the IFN-γ plus αPD-L1 group (figure 5A). The changes of $CD4^+$ T cells are shown in figure 5B, and show little correlation with the tumor growth. The $CD8^+$ /Treg ratios were found increased in IFN-γ+αPD-L1 group compared with that of αPD-L1 group (online supplemental figure S4A).

DISCUSSION

Although PD-1/PD-L1 checkpoint blockade therapies have been clinically used to treat advanced solid tumors, the objective response rate is still unsatisfactory.[32] To improve the low responsiveness of PD-1/PD-L1 inhibitors, more than 1700 clinical trials have been performed for combination therapies.[33] However, how to non-invasively guide the combination therapy remains a significant obstacle.[34]

Tumor PD-L1 overexpression has been recognized as one of the predictors for clinical effectiveness and better survival in patients treated with PD-1/PD-L1 inhibitors.[35] However, the PD-L1 expression during cancer progression and treatment is a dynamic process, thus it is impossible to monitor PD-L1 expression by traditional IHC. Moreover, PD-L1 levels determined by IHC might not represent the actual status due to the tumor heterogeneity.[16] In contrast, the non-invasive nuclear imaging of PD-L1 expression can determine the tumor PD-L1 levels in a real-time, dynamic and quantitative manner, which would be beneficial to guide the personalized combination therapies.[19] Until now, some efforts have been made for non-invasive imaging of tumor PD-L1 expression by PET or SPECT. Some radionuclide-labeled nanobodies have been applied for preclinical and early phase clinical research.[36–38] However, little attention has been paid to how to determine the therapeutic time window of PD-1/PD-L1 immunotherapy by non-invasive PD-L1-targeted imaging. We proposed that the period when the PD-L1 expression in tumors was high or upregulated as

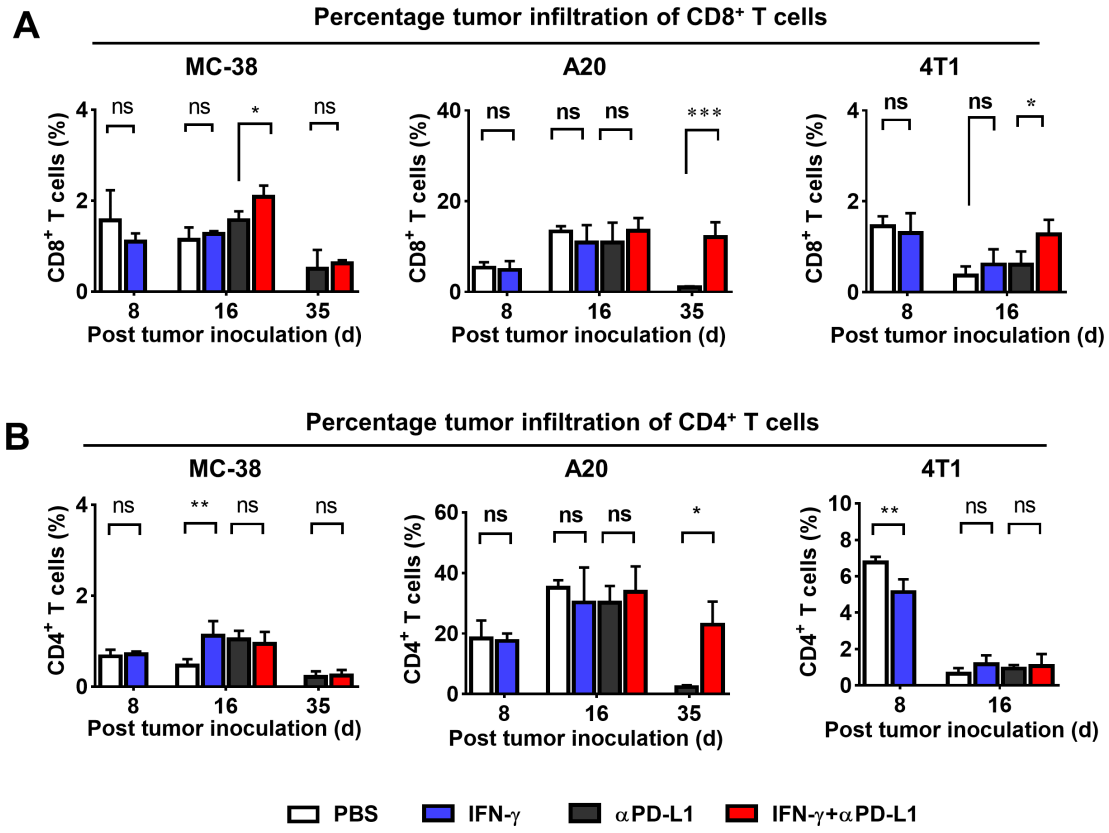

Figure 5 Analyzes of tumor infiltrating T cells. Percentage of (A) $CD8^+$ T cells and (B) $CD4^+$ T cells in the digested MC-38, A20 and 4T1 tumor cells after anti-PD-L1 therapy (n=4 to 6, mean±SD, *p<0.05, **p<0.01, ***p<0.001). αPD-L1, anti-programmed death ligand-1; d, days; IFN-γ, interferon-γ; PBS, phosphate-buffered saline.

determined by SPECT could be a favorable time window for initiation of immunotherapies. In this study, we developed a new radiolabeled PD-L1 targeted nanobody ^{99m}Tc-MY1523 to identify the crucial time window for PD-L1 blockade therapy.

Both in vitro and in vivo studies demonstrated a high specificity of ^{99m}Tc-MY1523 to PD-L1. The competitive binding assay revealed the different binding epitopes between MY1523 and the αPD-L1 antibody (figure 1A). Therefore, ^{99m}Tc-MY1523 could detect the tumor PD-L1 expression during immunotherapy with the αPD-L1 antibody and could provide guidance for multidose regimens. The results from SPECT/CT and biodistribution studies showed high tumor uptake of ^{99m}Tc-MY1523 in the mice bearing MC-38, A20 and 4T1 tumors at 2 hours p.i. The in vivo specificity of ^{99m}Tc-MY1523 was very similar to those radiolabel therapeutic antibodies,[23 39] and the PD-L1 overexpression in normal brown adipose tissue[40] also led to apparently high uptake of ^{99m}Tc-MY1523. Moreover, SPECT/CT showed a favorable contrast of ^{99m}Tc-MY1523 as early as 1 to 2 hours p.i. between the tumor and normal tissue, whereas it typically took 1 to 3 days for antibody-based imaging probes.[41] Thus, nanobody-based radiotracers are more convenient for clinical use. We also demonstrated a good correlation between the tumor uptake of ^{99m}Tc-MY1523 and the PD-L1 expression either on DCs or tumor cells. ^{99m}Tc-MY1523 is feasible for determination of PD-L1 expression by SPECT/CT in a real time, dynamic and quantitative manner. Since we completed the immunotherapy experiments in mice, we used a nanobody MY1523 that recognized mouse PD-L1.

In addition, we also prepared a nanobody probe ^{99m}Tc-NB17 that recognized human PD-L1 and performed imaging studies in nude mouse tumor models bearing human tumor xenografts (online supplemental figure S7). The results showed that the NCI-H226 (PD-L1-positive) tumors could be clearly visualized, while the HT-29 (PD-L1-negative) tumors could not be visualized. We believe that ^{99m}Tc-NB17 would be a promising radiotracer for clinical translation, and we are preparing ethical applications for clinical imaging of PD-L1 and guiding clinical αPD-L1 immunotherapy. Although we compared the tracers with or without Ni-Nitrilotriacetic acid (NTA) column purification for the in vivo behavior in mice model, and did not find a significant difference, the Ni-NTA column purification process is required for the clinical translation studies of the human PD-L1 reactive nanobody. We are also developing new labeling methods for the nanobodies, including the use of the Sortase-A system to prepare radiolabeled precursors. For example, the 'click chemistry' group N_3 is introduced into the nanobody via GGGG-N_3, then the purified nanobody-N_3 is obtained through Ni-NTA column purification. The Dibenzocyclooctyne (DBCO)-coupled bifunctional chelating agent is used for the radiolabeling, and the radiolabeled nanobody is prepared by a click chemistry

method with relatively high coupling efficiency. This method can also reduce the presence of various radioactive and non-radioactive impurities.

IFN-γ plays an important role in biological functions of nearly all immune cells, as well as innate and adaptive immune responses.[42] IFN-γ is a critical cytokine to change tumor PD-L1 expression,[43] and can upregulate the tumor PD-L1 expression through JAK-STAT pathway.[44] We thus used IFN-γ as an intervention means to establish tumor models with different PD-L1 levels and investigated the role of ^{99m}Tc-MY1523 SPECT/CT in detecting dynamic changes of PD-L1 expression. The results clearly showed that the PD-L1 expression in MC-38, A20 and 4T1 tumors after IFN-γ intervention was upregulated (figures 2C and 3B). Importantly, although IFN-γ intervention alone expedited the MC-38 tumor growth, the imaging-guided PD-L1 blockade therapy after IFN-γ intervention, which initiated during the time window, remarkably improved the therapeutic efficacy. The IFN-γ intervention had different impact on A20 and 4T1 tumor growth compared with the MC-38 tumor growth (figures 3C and 4A,C), but imaging-guided therapies after IFN-γ intervention also remarkably improved the therapeutic efficacy. Especially, the 4T1 tumors are not sensitive to PD-L1 blockade therapy;[30 31] however, this strategy of upregulating PD-L1 expression followed by imaging-guided PD-L1 blockade therapy could still result in a favorable antitumor efficacy and prolonged mice survivals, which has significant clinical values for the patients who have no or less response to the PD-L1 blockade therapy.

Recent reports showed that the PD-L1 expression on DCs was more important than on tumor cells in the response to PD-L1 blockade therapy.[45 46] Our study showed that the increased PD-L1 expression was from both DCs and tumor cells, while most of them came from DCs (figure 2D). Since the PD-L1 expression on 4T1 tumor cells is low,[47] IFN-γ intervention did not induce significant upregulation of PD-L1 expression on 4T1 tumor cells. Thus, the upregulated PD-L1 expression on DCs lead the main response to the PD-L1 blockade therapy in mice bearing 4T1 tumors.

One of the pivotal factors for immunotherapy effect are the infiltration of $CD8^+$ T cells into tumor tissues, and the ratio of $CD8^+$/Treg also reflects the effectiveness of treatment. Our results showed that infiltration of $CD8^+$ T cells (figure 5 and online supplemental figure S6) as well as $CD8^+$/Treg ratios (online supplemental figure S4) increased to varying degrees after treatment, which was consistent with the therapeutic outcome. Also, the higher degree of $CD8^+$ T-cell infiltration was associated with a longer median survival time (online supplemental figure S8).

The traditional cancer therapies, such as radiotherapy and chemotherapy, can remodel a 'hot' tumor microenvironment by favoring maturation of antigen-presenting cells, augmenting MHC-I dependent tumor antigen presentation and increasing tumor infiltration of $CD8^+$ T cells,[48] and can also increase tumor PD-L1 expression.[49 50] In fact, the combination of PD-L1 blockade therapy with radiotherapy or chemotherapy has been already applied in clinical practice. The strategy reported in this study would be rather essential for the better management of combination therapies.

CONCLUSION

The timing for PD-L1 blockade therapy is crucial due to dynamic expression of PD-L1 in tumors. This is a proof-of-concept study that proposed the time window determined by SPECT/CT imaging for the enhanced PD-L1 blockade immunotherapy of cancer, and the experimental results testified the hypothesis. We believe that the imaging-guided PD-L1 blockade therapy combined with radiotherapy or chemotherapy would possess significant clinical values, not only for the patients with response to further enhance the efficacy, but also for the patients with no or less response to obtain therapeutic effectiveness. We have already prepared the probe targeting human PD-L1, and the translational clinical study will be carried out in the near future.

Funding This work was supported in part by the National Natural Science Foundation of China (81630045, 81427802, 81927802, 81971676, 81671747, 81873907 and 81920108020), the National Key R&D Program of China (2018YFC1313300, 2017YFA0205600, and 2018YFE0205300), the Strategic Priority Research Program of the Chinese Academy of Sciences (XDA12020110) and the Beijing Natural Science Foundation (JQ19026 and L172007).

Competing interests None declared.

Patient consent for publication Not required.

Ethics approval All animal experiments were performed in accordance with the Institutional Animal Care and Use Committee (IACUC) at Peking University.

Provenance and peer review Not commissioned; externally peer-reviewed.

Data availability statement All data relevant to the study are included in the article or uploaded as supplementary information. All data relevant to the study are included in the article or uploaded as supporting information.

ORCID iD

Jiyun Shi http://orcid.org/0000-0001-7220-9637

REFERENCES

1 Gong J, Chehrazi-Raffle A, Reddi S, *et al*. Development of PD-1 and PD-L1 inhibitors as a form of cancer immunotherapy: a comprehensive review of registration trials and future considerations. *J Immunother Cancer* 2018;6:8.

2 Shen X, Zhao B. Efficacy of PD-1 or PD-L1 inhibitors and PD-L1 expression status in cancer: meta-analysis. *BMJ* 2018;362:k3529.
3 Carretero-González A, Lora D, Ghanem I, *et al*. Analysis of response rate with anti PD1/PD-L1 monoclonal antibodies in advanced solid tumors: a meta-analysis of randomized clinical trials. *Oncotarget* 2018;9:8706–15.
4 Lipson EJ, Forde PM, Hammers H-J, *et al*. Antagonists of PD-1 and PD-L1 in cancer treatment. *Semin Oncol* 2015;42:587–600.
5 Sambi M, Bagheri L, Szewczuk MR. Current challenges in cancer immunotherapy: multimodal approaches to improve efficacy and patient response rates. *J Oncol* 2019;2019:4508794
6 Gibbons Johnson RM, Dong H. Functional expression of programmed Death-Ligand 1 (B7-H1) by immune cells and tumor cells. *Front Immunol* 2017;8:961.
7 Alsaab HO, Sau S, Alzhrani R, *et al*. Pd-1 and PD-L1 checkpoint signaling inhibition for cancer immunotherapy: mechanism, combinations, and clinical outcome. *Front Pharmacol* 2017;8:561.
8 Yi M, Jiao D, Xu H, *et al*. Biomarkers for predicting efficacy of PD-1/PD-L1 inhibitors. *Mol Cancer* 2018;17:129.
9 Chen Q, Li T, Yue W. Drug response to PD-1/PD-L1 blockade: based on biomarkers. *Onco Targets Ther* 2018;11:4673–83.
10 Jørgensen JT, Hersom M. Companion diagnostics—a tool to improve pharmacotherapy. *Ann. Transl. Med.* 2016;4:482.
11 Tibaldi C, Lunghi A, Baldini E. Use of programmed cell death protein ligand 1 assay to predict the outcomes of non-small cell lung cancer patients treated with immune checkpoint inhibitors. *World J Clin Oncol* 2017;8:320–8.
12 Shen X, Zhang L, Li J, *et al*. Recent findings in the regulation of programmed death ligand 1 expression. *Front Immunol* 2019;10:1337.
13 Kordbacheh T, Honeychurch J, Blackhall F, *et al*. Radiotherapy and anti-PD-1/PD-L1 combinations in lung cancer: building better translational research platforms. *Ann Oncol* 2018;29:301–10.
14 Hansen AR, Siu LL. Pd-L1 testing in cancer: challenges in companion diagnostic development. *JAMA Oncol* 2016;2:15–16.
15 Chamoto K, Hatae R, Honjo T. Current issues and perspectives in PD-1 blockade cancer immunotherapy. *Int J Clin Oncol* 2020;25:790–800.
16 Ilie M, Hofman V, Dietel M, *et al*. Assessment of the PD-L1 status by immunohistochemistry: challenges and perspectives for therapeutic strategies in lung cancer patients. *Virchows Arch* 2016;468:511–25.
17 Kerr KM, Hirsch FR. Programmed death ligand-1 immunohistochemistry: friend or foe? *Arch Pathol Lab Med* 2016;140:326–31.
18 Davis AA, Patel VG. The role of PD-L1 expression as a predictive biomarker: an analysis of all US food and drug administration (FDA) approvals of immune checkpoint inhibitors. *J Immunother Cancer* 2019;7:278.
19 Broos K, Lecocq Q, Raes G, *et al*. Noninvasive imaging of the PD-1:PD-L1 immune checkpoint: Embracing nuclear medicine for the benefit of personalized immunotherapy. *Theranostics* 2018;8:3559–70.
20 England CG, Ehlerding EB, Hernandez R, *et al*. Preclinical pharmacokinetics and biodistribution studies of 89Zr-labeled pembrolizumab. *J Nucl Med* 2017;58:162–8.
21 Josefsson A, Nedrow JR, Park S, *et al*. Imaging, biodistribution, and dosimetry of Radionuclide-Labeled PD-L1 antibody in an immunocompetent mouse model of breast cancer. *Cancer Res* 2016;76:472–9.
22 Cole EL, Kim J, Donnelly DJ, *et al*. Radiosynthesis and preclinical PET evaluation of 89Zr-nivolumab (BMS-936558) in healthy non-human primates. *Bioorg Med Chem* 2017;25:5407–14.
23 Hettich M, Braun F, Bartholomä MD, *et al*. High-Resolution PET imaging with therapeutic antibody-based PD-1/PD-L1 checkpoint tracers. *Theranostics* 2016;6:1629–40.
24 Mayer AT, Natarajan A, Gordon SR, *et al*. Practical Immuno-PET radiotracer design considerations for human immune checkpoint imaging. *J Nucl Med* 2017;58:538–46.
25 Vaneycken I, D'huyvetter M, Hernot S, *et al*. Immuno-imaging using nanobodies. *Curr Opin Biotechnol* 2011;22:877–81.
26 Chakravarty R, Goel S, Cai W. Nanobody: the "magic bullet" for molecular imaging? *Theranostics* 2014;4:386–98.
27 Yang EY, Shah K. Nanobodies: next generation of cancer diagnostics and therapeutics. *Front Oncol* 2020;10:1182.
28 Crauwels M, Massa S, Martin C, *et al*. Site-Specific radioactive labeling of nanobodies. *Methods Mol Biol* 2018;1827:505–40.
29 Garcia-Diaz A, Shin DS, Moreno BH, *et al*. Interferon receptor signaling pathways regulating PD-L1 and PD-L2 expression. *Cell Rep* 2017;19:1189–201.
30 Tang H, Wang Y, Chlewicki LK, *et al*. Facilitating T cell infiltration in tumor microenvironment overcomes resistance to PD-L1 blockade. *Cancer Cell* 2016;29:285–96.
31 Grasselly C, Denis M, Bourguignon A, *et al*. The antitumor activity of combinations of cytotoxic chemotherapy and immune checkpoint inhibitors is model-dependent. *Front Immunol* 2018;9:2100.
32 Chen L, Han X. Anti-Pd-1/Pd-L1 therapy of human cancer: past, present, and future. *J Clin Invest* 2015;125:3384–91.
33 Tang J, Yu JX, Hubbard-Lucey VM, *et al*. Trial Watch: the clinical trial landscape for PD1/PDL1 immune checkpoint inhibitors. *Nat Rev Drug Discov* 2018;17:854–5.
34 Khair DO, Bax HJ, Mele S, *et al*. Combining immune checkpoint inhibitors: established and emerging targets and strategies to improve outcomes in melanoma. *Front Immunol* 2019;10:453.
35 Aguiar PN, De Mello RA, Hall P, *et al*. Pd-L1 expression as a predictive biomarker in advanced non-small-cell lung cancer: updated survival data. *Immunotherapy* 2017;9:499–506.
36 Lecocq Q, Zeven K, De Vlaeminck Y, *et al*. Noninvasive imaging of the immune checkpoint LAG-3 using nanobodies, from development to pre-clinical use. *Biomolecules* 2019;9:548.
37 Xing Y, Chand G, Liu C, *et al*. Early Phase I Study of a ^{99m}Tc-Labeled Anti-Programmed Death Ligand-1 (PD-L1) Single-Domain Antibody in SPECT/CT Assessment of PD-L1 Expression in Non-Small Cell Lung Cancer. *J Nucl Med* 2019;60:1213–20.
38 Broos K, Lecocq Q, Xavier C, *et al*. Evaluating a single domain antibody targeting human PD-L1 as a nuclear imaging and therapeutic agent. *Cancers* 2019;11:872.
39 Nedrow JR, Josefsson A, Park S, *et al*. Pharmacokinetics, microscale distribution, and dosimetry of alpha-emitter-labeled anti-PD-L1 antibodies in an immune competent transgenic breast cancer model. *EJNMMI Res* 2017;7:57.
40 Ingram JR, Dougan M, Rashidian M, *et al*. Pd-L1 is an activation-independent marker of brown adipocytes. *Nat Commun* 2017;8:647.
41 Warram JM, de Boer E, Sorace AG, *et al*. Antibody-Based imaging strategies for cancer. *Cancer Metastasis Rev* 2014;33:809–22.
42 Miller CHT, Maher SG, Young HA. Clinical use of interferon-gamma. *Ann N Y Acad Sci* 2009;1182:69–79.
43 Jiang X, Wang J, Deng X, *et al*. Role of the tumor microenvironment in PD-L1/PD-1-mediated tumor immune escape. *Mol Cancer* 2019;18:10.
44 Mimura K, Teh JL, Okayama H, *et al*. Pd-L1 expression is mainly regulated by interferon gamma associated with JAK-STAT pathway in gastric cancer. *Cancer Sci* 2018;109:43–53.
45 Tang H, Liang Y, Anders RA, *et al*. Pd-L1 on host cells is essential for PD-L1 blockade–mediated tumor regression. *J Clin Invest* 2018;128:580–8.
46 Lin H, Wei S, Hurt EM, *et al*. Host expression of PD-L1 determines efficacy of PD-L1 pathway blockade-mediated tumor regression. *J Clin Invest* 2018;128:805–15.
47 Sagiv-Barfi I, Kohrt HEK, Czerwinski DK, *et al*. Therapeutic antitumor immunity by checkpoint blockade is enhanced by ibrutinib, an inhibitor of both Btk and Itk. *Proc Natl Acad Sci U S A* 2015;112:E966–72.
48 Lazzari C, Karachaliou N, Bulotta A, *et al*. Combination of immunotherapy with chemotherapy and radiotherapy in lung cancer: is this the beginning of the end for cancer? *Ther Adv Med Oncol* 2018;10:1758835918762094.
49 Gong J, Le TQ, Massarelli E, *et al*. Radiation therapy and PD-1/PD-L1 blockade: the clinical development of an evolving anticancer combination. *J Immunother Cancer* 2018;6:46.
50 Ng HY, Li J, Tao L, *et al*. Chemotherapeutic treatments increase PD-L1 expression in esophageal squamous cell carcinoma through EGFR/ERK activation. *Transl Oncol* 2018;11:1323–33.

Nuclear Imaging-Guided PD-L1 Blockade Therapy Increases Effectiveness of Cancer Immunotherapy

Hannan Gao[1#], Yue Wu[1#], Jiyun Shi[2#], Xin Zhang[1], Tianyu Liu[1], Biao Hu[1], Bing Jia[1], Yakun Wan[3], Zhaofei Liu[1], and Fan Wang[1,2,4]*

[1] Medical Isotopes Research Center and Department of Radiation Medicine, State Key Laboratory of Natural and Biomimetic Drugs, School of Basic Medical Sciences, Peking University, Beijing 100191, China

[2] Key Laboratory of Protein and Peptide Pharmaceuticals, CAS Center for Excellence in Biomacromolecules, Institute of Biophysics, Chinese Academy of Sciences, Beijing 100101, China

[3] Shanghai Novamab Biopharmaceuticals Co., Ltd., Shanghai 201318, China

[4] Bioland Laboratory (Guangzhou Regenerative Medicine and Health Guangdong Laboratory), Guangzhou 510005, China.

Running title: Nuclear imaging-guided PD-L1 blockade immunotherapy

[#]These authors contributed equally to this work.

*For correspondence contact: Fan Wang, Medical Isotopes Research Center, Peking University, Beijing 100191, China. E-mail: wangfan@bjmu.edu.cn

This file contains:

1. Supplementary Materials and Methods.
2. Supplementary Results
3. Supplementary Figures 1-8 and their legends.

SUPPLEMENTARY MATERIALS AND METHODS

Materials

The human PD-L1-targeted nanobody NB17, which has a LPETG-His_6 tag on the C-terminus, was provided by Novamab Biopharmaceuticals Co., Ltd. (Shanghai, China).

Cells and animal models.

The HT-29 (human colon cancer) and NCI-H226 (human lung cancer) cell lines were purchased from the American Type Culture Collection (Manassas, VA, USA). Both cells were cultured in RPMI-1640 with 10% fetal bovine serum (FBS) in a humidified atmosphere with 5% CO_2 at 37 ℃. To verified cell PD-L1 expression, NCI-H226 and HT-29 cells were stained with hPD-L1 (1 Cat. No. 374509, 1 μg/mL) at 4°C for 30 min for flow cytometry. To prepare HT-29 or NCI-H226 tumor models, 5 x 10^6 cells were incubated subcutaneously into the right flank of female BALB/c nude mice (4~5 week age).

Radiochemistry of ^{99m}Tc-HYNIC-G_4K

The radiochemical yield (RCY) of ^{99m}Tc-HYNIC-G_4K was determined by an Agilent 1260 Infinity High Performance Liquid Chromatography (HPLC) system equipped with a radioactive detector (Gabi star, raytest, Germany). The radiotracers were analyzed by a C_{18} column (Agilent Xorbax SB-C18, 4.6 mm × 250 mm, 5 μm). The mobile phase was comprised of solvent A (0.05 % TFA in water) and solvent B (0.05% TFA in acetonitrile). The flow rate was 1 mL/min. The gradient of solvent B started with 10 % at 0 min to 50 % at 20 min.

Radiochemistry of ^{99m}Tc-MY1523

^{99m}Tc-MY1523 was prepared by mixture of Sortase-A, MY1523 and ^{99m}Tc-HYNIC-G_4K. The mass ratio of (^{99m}Tc)-HYNIC-G_4K and the nanobody was 3: 100 (molar ratio was 1:1.5). Sortase-A was using a 17 kDa reactive short sequence: MHHHHHHAKP QIPKDKSKVA GYIEIPDADI EPVYPGPAT SEQLNRGVSF AEENESLDDQ NISIA.

The radiochemical yield (RCY) of ^{99m}Tc-MY1523 was determined by instant thin-layer chromatography (ITLC) on ITLC-SG (Agilent, USA, 5 mm x 90 mm), developed in saline and detected via a radio-TLC imaging scanner (Bioscan, AR-2000, USA) (Rf = 0 ~ 0.3 for ^{99m}Tc-HYNIC-G_4K and free ^{99m}Tc, Rf = 0.7 ~ 1.0 for ^{99m}Tc-MY1523). After purification by high-performance size exclusion chromatography (HPSEC) with a Superose-12 (10 mm x 300 mm, GE Healthcare Life Science) or Superdex-75 (Increase 10/300 GL, GE Healthcare Life Science) column, and PBS (pH = 7.2~7.4) containing 0.1% Tween-20 as eluent at a flow rate of 0.8 mL/min, the final product was collected and determined for the radiochemical purity (RCP) by ITLC. Then, the in vitro stability of ^{99m}Tc-MY1523 injection was determined at room temperature at 6 h. The RCP of ^{99m}Tc-MY1523 was also determined by HPSEC and SDS-PAGE. SDS-PAGE was using 2 MBq ^{99m}Tc-MY1523. It was imaged by SPECT (peak: 140 keV, 20%), and metal markers matched with the pre-stained protein markers were set for CT signal (50 kVp). The SPECT and CT images were merged for SPECT/CT imaging.

Cell binding assays of ^{99m}Tc-MY1523

The binding affinity of ^{99m}Tc-MY1523 was determined on A20 cells. Briefly, 10^6 cells were incubated in 100 μL PBS containing 2% FBS, 37 kBq ^{99m}Tc-MY1523 (3.7

kBq/ng) and a gradient of cold MY1523 (0.1 nM~100 μM) on ice for 2 h. Cells were collected by a refrigerated centrifuge (500 x g for 5 min). After washes with cold PBS, cells were suspended in 500 μL PBS and counted for radioactivity via a γ-counter (PerkinElmer Inc., USA). The best-fit 50% inhibitory concentration (IC50) values were analyzed using Prism v7.0. Experiments were performed with 4 duplicates.

Flow cytometry

For analyzing T cell infiltration in the tumor microenvironment (TME), tumors were digested cells were incubated with cocktailed antibodies containing CD45 (1 μg/mL, Cat. 56-0451-82, eBioscience), CD3e (1 μg/mL, Cat. 25-0031-82, eBioscience), CD4 (1 μg/mL, Cat. 45-0042-82, eBioscience) and CD8 (2.5 μg/mL, Cat. 11-0081-82, eBioscience) for 30 min. Foxp-3 staining was used the transcription factor staining buffer kits (Cat. 00-5523-00, eBioscience) and stained with Foxp3 (1 μg/mL, Cat. 12-4771-82, eBioscience) for 30 min. Samples were analyzed via a Gallios (Beckman Coulter, USA) flow cytometer.

For analyzing T cell activation in tumor draining lymph nodes (TDLN), they were excised and grinded on 80 μm sieve for lymphocyte suspension. Before staining, cells were incubated in RPMI-1640 medium with 10% FBS and Leukocyte Activation Cocktail with BD GolgiPlug™ (Cat.550583, BD, 2 μL/mL) at 37°C for 4 h. Cells were washed, suspended in cold PBS containing 2% FBS and stained dead cells using fixable dead cell stain kits (Cat. L34959, Invitrogen). Cells were stained with CD45 (1 μg/mL, Cat. 56-0451-82, eBioscience), CD8 (2.5 μg/mL, Cat. 11-0081-82, eBioscience) and IFN-γ (0.25 μg/mL Cat. 505821, Biolegend). Samples were analyzed via a Gallios (Beckman Coulter, USA) flow cytometer.

Protein binding assays of NB17

The binding affinity and specificity of NB17 was determined by hPD-L1 binding assays using recombinant human PD-L1 (Sino Biological Inc., Beijing, China) and ^{125}I- NB17. The protein binding assays was similar to that of ^{125}I-MY1523.

In vivo evaluation of ^{99m}Tc-NB17

The preparation, SPECT/CT imaging and biodistribution studies of ^{99m}Tc-NB17 are similar to that of ^{99m}Tc-MY1523. For SPECT/CT imaging, NCI-H226 and HT-29 tumor bearing mice were injected with 18 MBq ^{99m}Tc-NB17 and imaged at 1, 2 and 4 h p.i. For biodistribution studies, NCI-H226 and HT-29 tumor bearing mice were injected with 370 kBq ^{99m}Tc-NB17 and determined at 1, 2 and 4 h p.i. The blocking group was co-injected with 0.5 mg NB17 with the radiotracer.

SUPPLEMENTARY RESULTS

Radiochemistry of ^{99m}Tc-HYNIC-G$_4$K

The radiochemical yield (RCY) of ^{99m}Tc-HYNIC-G$_4$K was determined by RP-HPLC. The representative HPLC chromatogram of ^{99m}Tc-HYNIC-G$_4$K was shown in Fig. S2A. The RCY of ^{99m}Tc-HYNIC-G$_4$K was > 95%.

Radiochemistry of ^{99m}Tc-MY1523

The RCY of ^{99m}Tc-MY1523 was determined by ITLC. The representative ITLC chromatogram was shown in Fig. S2B. As results, 50% RCY was often obtained after the 2 steps in total. After purification, the radiochemical purity (RCP) of the final product was determined by ITLC. The representative ITLC chromatogram of ^{99m}Tc-MY1523 was shown in Fig. S2C. The RCP of end-product was > 99%. The

stability of ^{99m}Tc-MY1523 was determined in PBS at room temperature. As shown in Fig. S2D, ^{99m}Tc-MY1523 was stable for 6 h placement.

The RCP of ^{99m}Tc-MY1523 was also determined by HPGEC and SDS-PAGE. The representative HPGEC chromatogram was shown in Fig. S3A. The RCP of ^{99m}Tc-MY1523 was > 99%. The retention time of ^{99m}Tc-MY1523 was at 16.6 min, which was a little earlier than that of cold MY152 (17.3 min for MY1523). The representative radioactive SDS-PAGE was shown in Fig. S3B. The molecular weight of ^{99m}Tc-MY1523 was still around 15 kDa, close to that of cold MY1523. The final product contained ^{99m}Tc-MY1523 and cold MY1523 as carrier.

Cell binding Assays

The binding affinity of MY1523 was also determined on A20 cells using ^{99m}Tc-MY1523 as a radiotracer. The competitive binding assay of ^{99m}Tc-MY1523 was shown in Fig. S3C. The IC_{50} of MY1523 against ^{99m}Tc-MY1523 was determined to be 5.95 ± 0.71 nM.

Flow cytometry

Additional T cell analysis was determined at 16 d in MC-38 and 4T1 tumors. Regulatory T cell (Treg) analysis were shown in Fig. S4A. In MC-38 tumors, IFN-γ intervention increased the percentage of tumor Treg, and the CD8/Treg ratio was decreased comparing to that of the control group, which was consistent with that IFN-γ expedited the tumor growth. After the PD-L1 blockade therapy, the CD8/Treg ratio showed increased (not significant), resulting in tumor growth inhibition. In 4T1 tumors, the percentage of Treg and the CD8/Treg ratio showed no significant change by IFN-γ intervention. After PD-L1 blockade therapy, the CD8/Treg ratio significantly increased,

resulting in tumor growth inhibition. The percentage of activation of effector T cells in TDLN was shown in Fig. S4B. IFN-γ and αPD-L1 therapy decreased significantly IFN-γ^+ proportion in TDLN comparing to that of αPD-L1 therapy both in MC-38 and 4T1 tumor bearing mice. One possible explanation is that the activated T cells may infiltrate into tumor tissues from TDLN, therefore leading to the decrease of IFN-γ^+ population in $CD8^+$ T cells.

The gating strategies for tumor infiltrating T cells and activated effector T cells in TDLNs were shown in Fig. S5. The representative $CD8^+$ and $CD4^+$ density plots at day 16 were shown in Fig**.** S6. The percentage of $CD8^+$ in digested tumor cells was found increased in the combination group of IFN-γ plus αPD-L1 than that of αPD-L1 group in MC-38 and 4T1 tumors, while it was not significant in A20 tumors. The results showed that the percentage of $CD4^+$ T cells showed little significance.

The evaluation of ^{99m}Tc-NB17

The binding affinity of NB17 was determined by hPD-L1 binding assays using recombinant human PD-L1 (Sino Biological Inc., Beijing, China) and ^{125}I-NB17, which was similar to that of ^{125}I-MY1523. To verified cell PD-L1 expression, NCI-H226 and HT-29 cells were incubated in PBS containing 2% fetal bovine serum and hPD-L1 (Biolegend, Cat. No. 374509, 1 μg/mL) at 4 °C for 30 min. The cells were determined on a BD FACSCalibur flow cytometer. The preparation, SPECT/CT imaging and biodistribution studies of ^{99m}Tc-NB17 were similar to that of ^{99m}Tc-MY1523. For in vivo studies, cold NB17 was added into ^{99m}Tc-NB17 as carrier and the specific activity of ^{99m}Tc-NB17 was prepared as 18 MBq/100 μg. The in vivo behavior of ^{99m}Tc-NB17 were determined in NCI-H226 and HT-29 tumor bearing mice at 1 h p.i. The mice were injected with 18 MBq ^{99m}Tc-NB17 for SPECT/CT

imaging or 370 kBq ^{99m}Tc-NB17 for biodistribution studies. The blocking group mice were co-injected with 0.5 mg NB17 through the tail vein.

The binding affinity of NB17 was determined by hPD-L1 binding assays. NB17 showed a high affinity (KD = 3.79 ± 0.78 nM) to human PD-L1 (Fig. S7A). The PD-L1 expression on tumor cells were determined by flow cytometry, and the resulte showed that NCI-H226 was PD-L1-positive, while HT-29 was PD-L1-negative (Fig. S7B). The SPECT/CT imaging of ^{99m}Tc-NB17 in mice bearing NCI-H226 or HT-29 tumors were shown in Fig. S7C. At 1 h p.i., the PD-L1- positive NCI-H226 tumors could be clearly visualized, and the PD-L1-negative HT-29 tumors or the NCI-H226 tumors in the blocking group were barely visualized. The biodistribution results were similar to that of imaging studies. As shown in Fig. S7D, the NCI-H226 tumor uptake was significantly higher than that of HT-29 tumors (5.91 ± 0.71 vs. 0.80 ± 0.14 %ID/g, at 1 h p.i., $P < 0.0005$) or the blocking group (5.91 ± 0.71 vs. 1.25 ± 0.29 vs. %ID/g, at 1 h p.i., $P < 0.0001$). These results suggested that ^{99m}Tc-NB17 specifically binds to hPD-L1 in vivo and it could be a promising imaging probe for guiding immunotherapy clinically.

Supplementary Figures

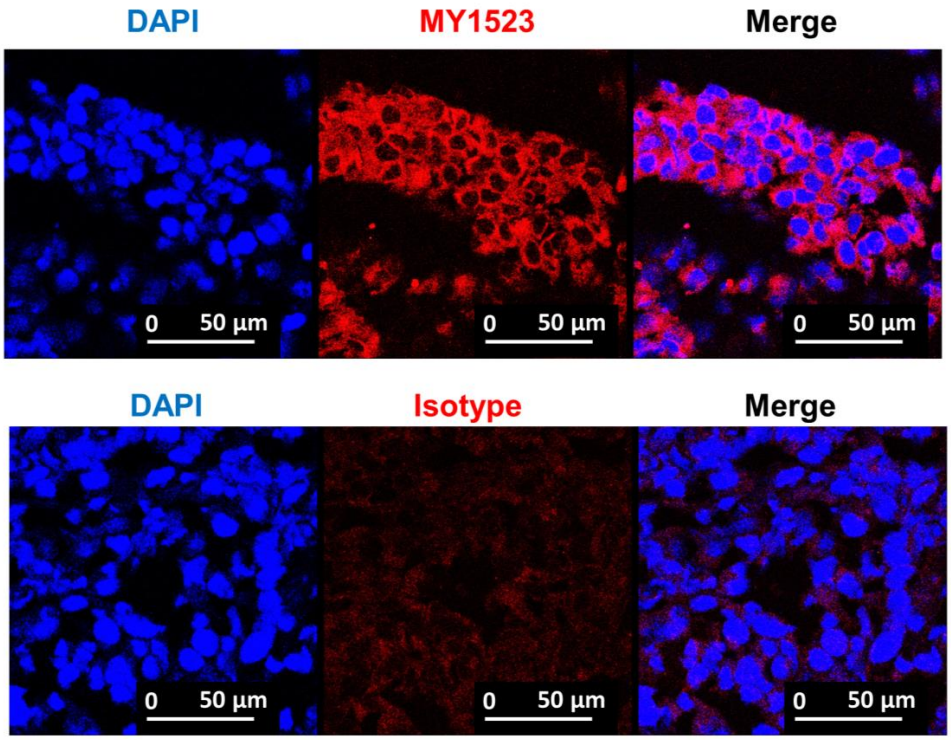

FIGURE S1. Immunofluorescence staining of MY1523 on MC-38 tumor sections. The isotype control used Mirc415, a nanobody targeting hPD-L2 with no cross reaction with mPD-L2.

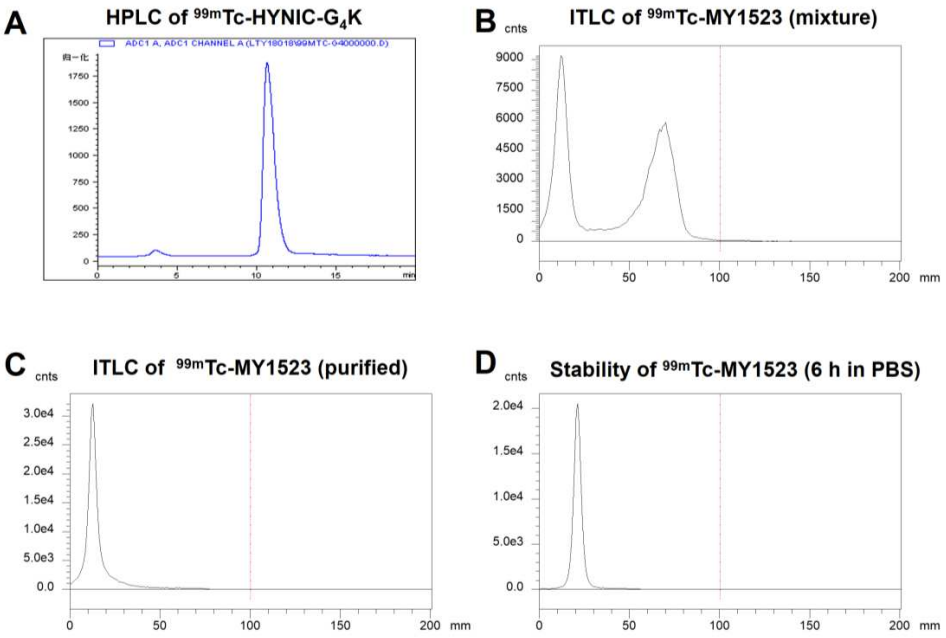

FIGURE S2. Radiochemistry of ^{99m}Tc-HYNIC-G_4K and ^{99m}Tc-MY1523. (A) Representative RP-HPLC chromatogram of ^{99m}Tc-HYNIC-G_4K. (B) Representative ITLC chromatograms of the ^{99m}Tc-MY1523 mixture and (C) the purified product of ^{99m}Tc-MY1523. (D) In vitro stability of ^{99m}Tc-MY1523 in PBS at 6 h.

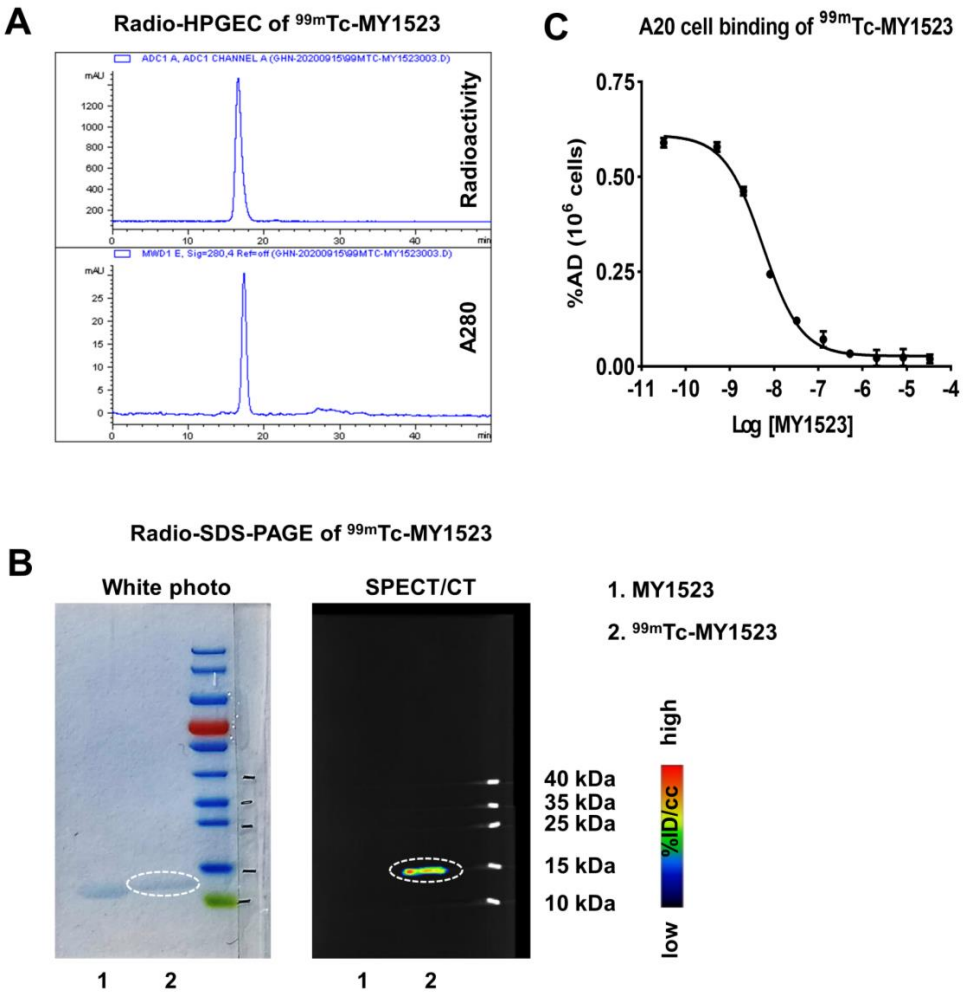

FIGURE S3. Radiochemistry of ^{99m}Tc-MY1523. (A) Representative HPSEC chromatogram of ^{99m}Tc-MY1523. (B) Coomassie stained SDS-PAGE gel and SPECT/CT imaging of ^{99m}Tc-MY1523 SDS-PAGE. (C) Competitive binding assay on A20 cells of ^{99m}Tc-MY1523 (n = 4, mean ± SD).

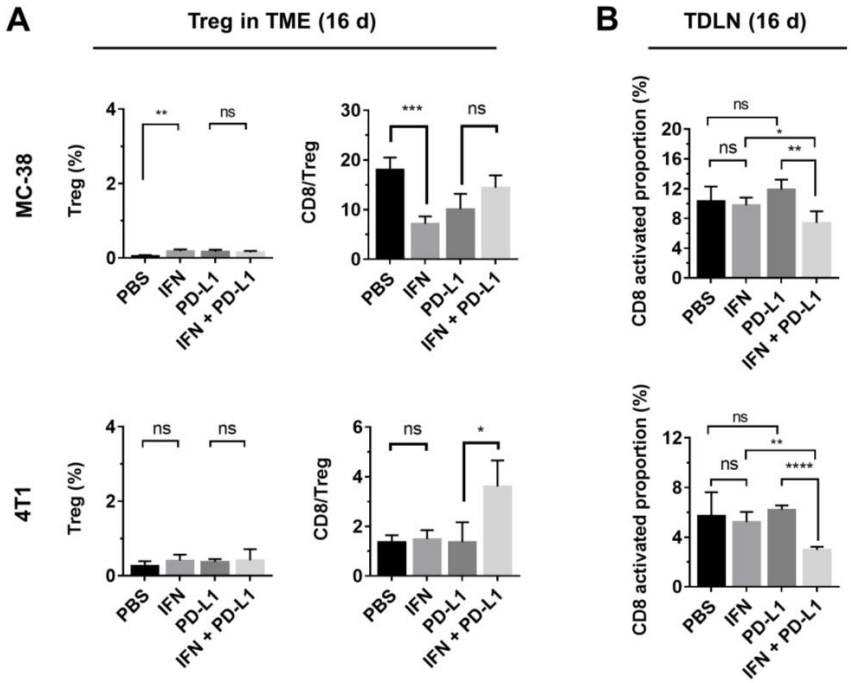

FIGURE S4. T-cell analyses at 16 d. (A) The percentage of Treg and the $CD8^+$/Treg ratios in TME (n = 4, mean ± SD, * $P < 0.05$, ** $P < 0.01$, *** $P < 0.001$). (B) The percentage of activated effector T cells in TDLNs (n = 4, mean ± SD, ** $P < 0.01$, **** $P < 0.0001$). TME: tumor microenvironment; TDLN: tumor draining lymph node.

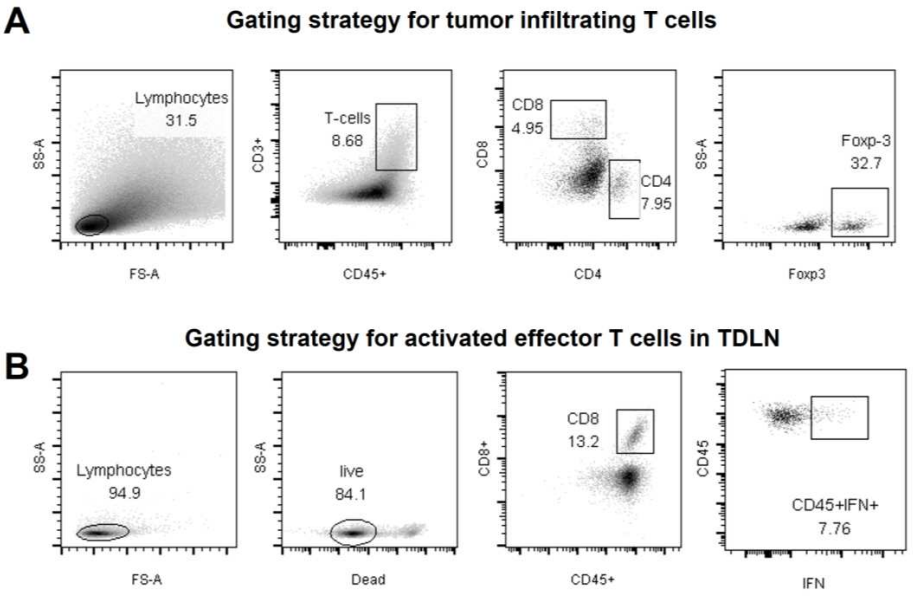

FIGURE S5. FACS gating strategy for T cells. (A) The gating strategy for $CD8^+$ T cells ($CD45^+CD3e^+CD8^+$), $CD4^+$ T cells ($CD45^+CD3e^+CD4^+$) and Treg ($CD45^+CD3e^+CD4^+Foxp\text{-}3^+$). (B) The gating strategy for activated effector T cells (Lived $CD45^+CD8^+$ IFN-γ^+).

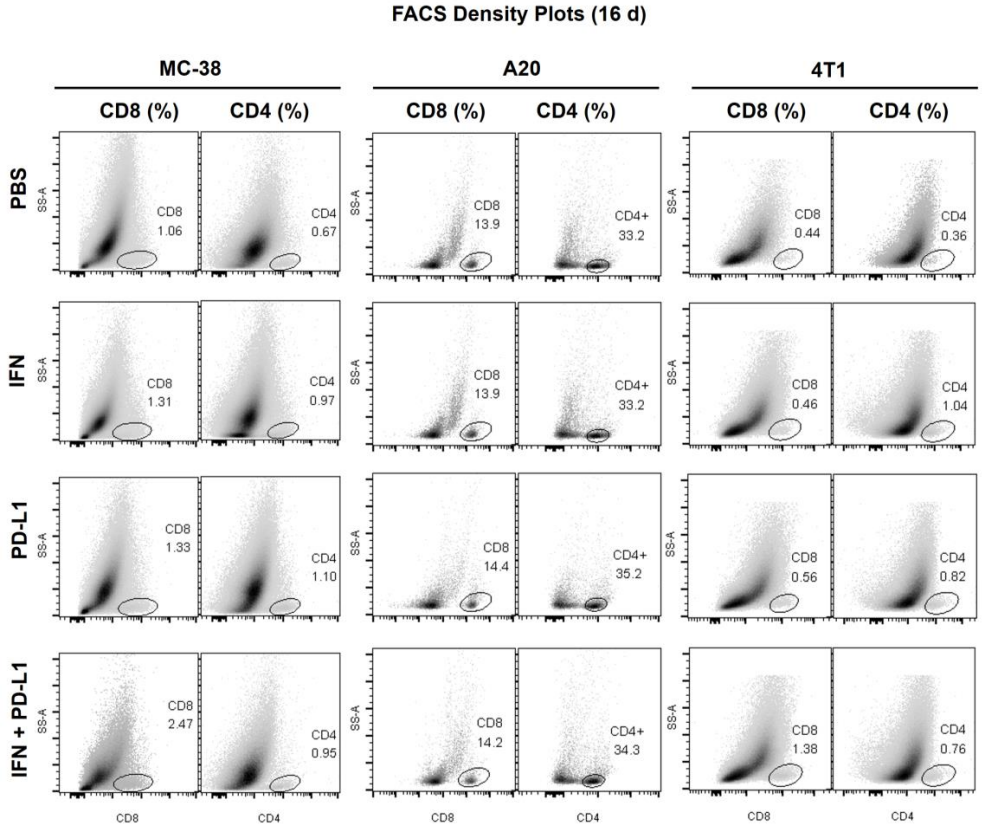

FIGURE S6. Representative $CD8^+$ and $CD4^+$ density plots for analyzing TILs at 16 d.

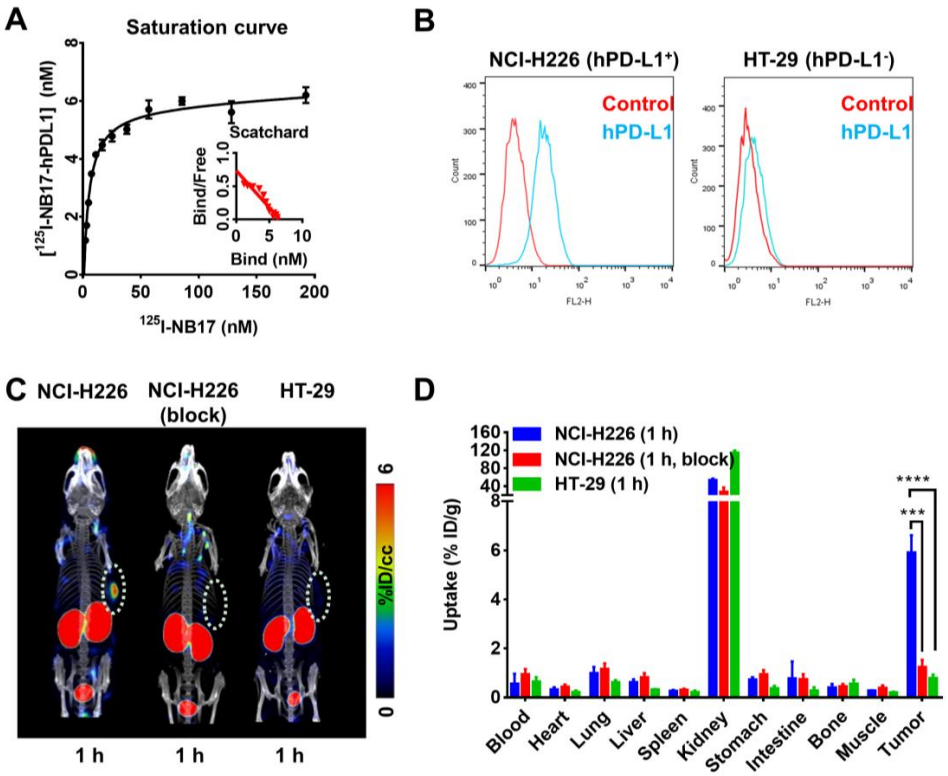

FIGURE S7. The evaluation of ^{99m}Tc-NB17 targeting to hPD-L1. (A) Human PD-L1 binding assays of ^{125}I-NB17. (B) PD-L1 expression on NCI-H226 and HT-29 cells. (C) SPECT/CT imaging and (D) biodistribution studies in mice bearing NCI-H226 or HT-29 tumors at 1 h p.i. (n = 4, mean ± SD, *** $P < 0.001$, **** $P < 0.0001$).

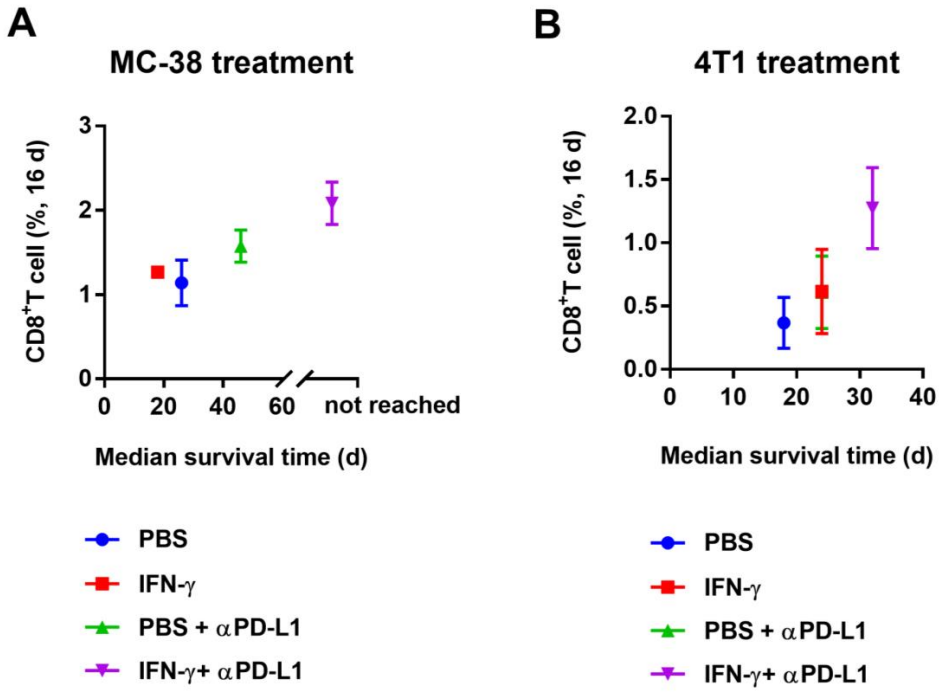

FIGURE S8. The correlation between median survival time and T cell infiltration at day 16 in MC-38 and 4T1 models.